Experience-dependent structural plasticity at pre- and postsynaptic sites of layer 2/3 cells in developing visual cortex

Yujiao Jennifer Sun[a,1], J. Sebastian Espinosa[a,1], Mahmood S. Hoseini[a], and Michael P. Stryker[a,2]

[a]Department of Physiology, Kavli Institute for Fundamental Neuroscience, University of California, San Francisco, CA 94143-0444

Contributed by Michael P. Stryker, September 5, 2019 (sent for review August 23, 2019; reviewed by Jianhua Cang and Joshua T. Trachtenberg)

The developing brain can respond quickly to altered sensory experience by circuit reorganization. During a critical period in early life, neurons in the primary visual cortex rapidly lose responsiveness to an occluded eye and come to respond better to the open eye. While physiological and some of the molecular mechanisms of this process have been characterized, its structural basis, except for the well-known changes in the thalamocortical projection, remains obscure. To elucidate the relationship between synaptic remodeling and functional changes during this experience-dependent process, we used 2-photon microscopy to image synaptic structures of sparsely labeled layer 2/3 neurons in the binocular zone of mouse primary visual cortex. Anatomical changes at presynaptic and postsynaptic sites in mice undergoing monocular visual deprivation (MD) were compared to those in control mice with normal visual experience. We found that postsynaptic spines remodeled quickly in response to MD, with neurons more strongly dominated by the deprived eye losing more spines. These postsynaptic changes parallel changes in visual responses during MD and their recovery after restoration of binocular vision. In control animals with normal visual experience, the formation of presynaptic boutons increased during the critical period and then declined. MD affected bouton formation, but with a delay, blocking it after 3 d. These findings reveal intracortical anatomical changes in cellular layers of the cortex that can account for rapid activity-dependent plasticity.

ocular dominance | critical period | cortical plasticity | cortical development | structural plasticity

Sensory experience during early life plays an instructive role in the formation and maturation of neural circuits (1–4). Abnormal experience within early critical periods has life-long effects (5–7). In the visual system, monocular visual deprivation (MD) within a critical period causes drastic changes in visual cortical responses in many species (8–12) that are highly stereotyped and reproducible. In the mouse, the effects of MD during the critical period take place in temporally and mechanistically distinct stages: a Hebbian-like process with decreased response to the deprived eye in the first 2 to 3 d (13), followed by a delayed increase in response to the open eye governed by both Hebbian and homeostatic rules (14–17). After reopening the deprived eye within the critical period, recovery of responses to normal levels occurs within 2 d (15, 18, 19).

Structural reorganization at various anatomical sites has also been described in association with the overall loss of response to the deprived eye. At thalamorecipient layer 4, remodeling of thalamic axonal arbors takes place over days to weeks [cat (20–23), mouse (24)]. Physiological changes beyond the input layer of cat visual cortex are much more rapid (25), and the reorganization of intracortical connections (26) in the extragranular layers has a similar time course to the rapid changes in physiological responses. These findings support the idea that synapses beyond layer 4 are the loci for rapid remodeling (25). In both the adult (27–32) and developing (33) visual cortex of the mouse, altered experience increases turnover of excitatory and inhibitory synapses in the superficial layers. Population studies of spines in layer 1 in vivo and spines in deeper layers in vitro have shown that prolonged dark rearing (34, 35) or MD (36, 37) decreases spine numbers in the visual cortex. However, the extent to which rewiring of upper-layer connections accounts for the functional changes in individual neurons remains unclear.

To answer this question, we studied synaptic remodeling longitudinally in individual neurons of the binocular zone of mouse visual cortex (V1) over the stages of ocular dominance plasticity during the critical period. We used 2-photon imaging to track the anatomical rearrangement of presynaptic boutons and postsynaptic spines within layer 2/3 excitatory neurons. Comparing the changes in control mice receiving normal visual input to those in experimental mice undergoing monocular deprivation and binocular recovery, we found that postsynaptic spines respond quickly to the altered visual experience and that this process is strongly correlated with the functional responses of individual cells. Presynaptic boutons also respond to altered visual experience but with a longer latency. The developmental increase in bouton formation was disrupted only after 3 d of MD.

Results

Labeling Synaptic Structures for Longitudinal Imaging. To study experience-dependent structural plasticity in the developing mouse visual cortex, we sparsely labeled layer 2/3 cortical excitatory neurons for longitudinal imaging. We used Cre-recombinase–dependent

Significance

The operation of the cortex depends on the connections among its neurons. Taking advantage of molecular and genetic tools to label major proteins of the presynaptic and postsynaptic densities, we studied how connections of layer 2/3 excitatory neurons in mouse visual cortex were changed by monocular visual deprivation during the critical period, which causes amblyopia. The deprivation induced rapid remodeling of postsynaptic spines and impaired bouton formation. Structural measurement followed by calcium imaging demonstrated a strong correlation between changes in postsynaptic structures and functional responses in individual neurons after monocular deprivation. These findings suggest that anatomical changes at postsynaptic sites serve as a substrate for experience-dependent plasticity in the developing visual cortex.

Author contributions: J.S.E. and M.P.S. designed research; J.S.E. performed research; Y.J.S. and M.S.H. analyzed data; and Y.J.S. and M.P.S. wrote the paper.

Reviewers: J.C., University of Virginia; and J.T.T., University of California, Los Angeles.

The authors declare no competing interest.

Data deposition: Puncta counter data have been deposited at https://github.com/ucsfidl/Puncta_Counter.

[1]Y.J.S. and J.S.E. contributed equally to this work.

[2]To whom correspondence may be addressed. Email: stryker@phy.ucsf.edu.

First published October 7, 2019.

plasmids with GFP fused to proteins that are abundant presynaptically (synaptophysin, SYP) or postsynaptically (the 95 kDa postsynaptic density protein, PSD95) to mark pre- and postsynaptic structures in individual neurons. To allow long-term visualization of these structures in layer 2/3 excitatory neurons in vivo, either PSD95-GFP or SYP-GFP plasmids were delivered together with Cre-recombinase into embryonic day 16 (E16) embryos of Ai14 mice, which conditionally express tdTomato (Fig. 1*A*). A Cre-dependent tdTomato construct was coelectroporated to enhance the brightness of the red channel. A cranial window with a cover glass was implanted over the primary visual cortex 4–7 d before the structural imaging, and intrinsic signal imaging was first carried out to identify the binocular zone (Fig. 1*B*). Around the peak of the critical period, near postnatal day 28 (P28) (10),

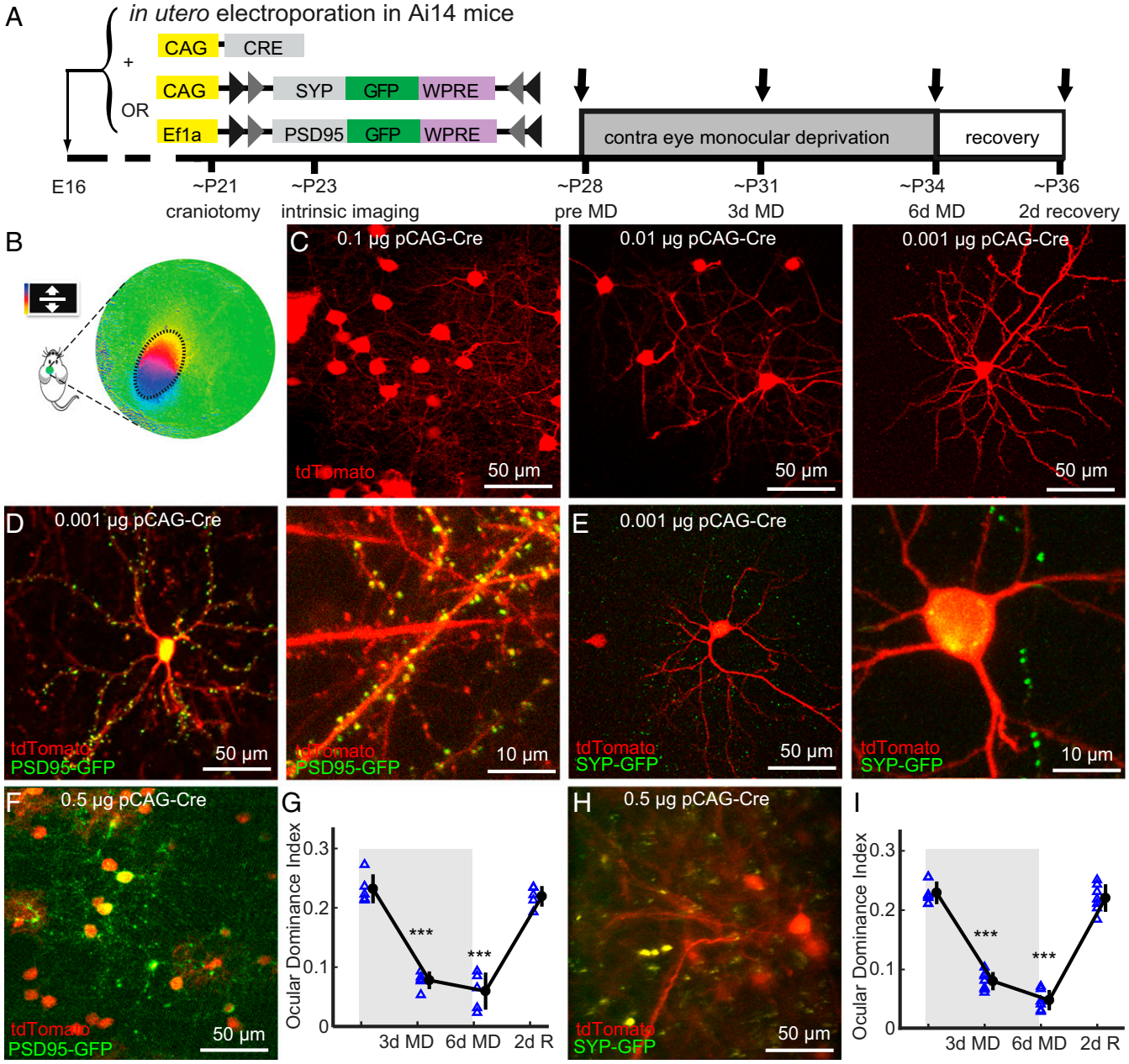

Fig. 1. Labeling of synaptic markers does not affect functional changes during MD. (*A*) Timeline of experiments: at E16, plasmids (pCAG-Cre and double floxed markers, either SYP-GFP or PSD95-GFP) were delivered into left ventricle in Ai14 embryos. After craniotomy P22–25, cortex was first screened for sparse neuronal labeling. Intrinsic imaging was then used to determine the exact location of the binocular zone of primary visual cortex. MD of experimental animals was performed by suture of contralateral eyelid P25–29 and lasted for 6 d. Structural imaging was performed at times indicated by arrows. (*B*) Example of intrinsic signal imaging to identify binocular zone of visual cortex. (*C*) Different dosages of pCAG-Cre plasmid delivered in Ai14 animals through in utero electroporation were tested for sparse labeling; 0.001 μg/μL pCAG-Cre was chosen for structural imaging. (*D*) Coexpression of pCAG-Cre and double floxed postsynaptic marker PSD95-GFP labeled cell bodies and neurite structure in red channel and postsynaptic structures in green channel. (*E*) Similar to *D* but for presynaptic marker SYP-GFP. (*F*) Overexpression of Cre (0.5 μg/μL) and PSD95-GFP (0.75 μg/μL) in Ai14 mice resulted in high-density labeling of cells and postsynaptic marker PSD95-GFP. (*G*) Intrinsic signal imaging demonstrated normal ODI shift with PSD95-GFP overexpression; each represents a single animal. (*H* and *I*) Similar to *F* and *G* but for presynaptic marker, overexpression of Cre and SYP-GFP in Ai14 animals resulted in normal ODI shift. Error bar represents mean ± SD ***$P < 0.001$ compared with the baseline (day 0) response (1-way ANOVA followed by multiple comparisons with Tukey's method).

we used 2-photon microscopy to track longitudinal changes in individual spines or boutons of cortical neurons in animals experiencing normal vision or MD.

To achieve the sparse labeling, a range of pCAG-Cre concentrations was delivered to Ai14 mouse embryos in which all neurons contain floxed tdTomato (Fig. 1*C*). A low concentration of the plasmid expressing Cre-recombinase (0.001 μg) yielded sparse labeling of individual neurons and was used for longitudinal structural imaging. The sparsely labeled layer 2/3 neurons were marked with red tdTomato fluorescence in their cell bodies, dendrites, and axons. Mixing the low concentration of recombinase plasmid with a higher concentration of the plasmid encoding either SYP-GFP or PSD95-GFP ensured that pre- or postsynaptic structures were also labeled with GFP in all of the red neurons. Neurons with PSD95-GFP labeling express bright fluorescent puncta within individual spines viewed using 2-photon imaging (Fig. 1*D*). In neurons with SYP-GFP labeling, presynaptic boutons are evident as isolated puncta on the axons marked with red fluorescence (Fig. 1*E*).

GFP-Tagged Synaptic Markers Do Not Impair Ocular Dominance Plasticity. A control experiment was carried out to confirm that the GFP-labeled synaptic markers did not alter the normal functional plasticity of mouse visual cortex. We labeled layer 2/3 neurons densely rather than sparsely with PSD95-GFP or SYP-GFP and measured ocular dominance plasticity using intrinsic signal imaging (Fig. 1*B*). Ocular dominance plasticity during MD and recovery phases was unaffected even by the 500-fold higher labeling of postsynaptic (Fig. 1*G*) or presynaptic (Fig. 1*I*) sites than was used in the experimental conditions (15, 16).

Image Processing Pipeline and Semiautomated Puncta Detection. In many cases, up to 9 overlapping volume image stacks were acquired in the same imaging session to capture a labeled neuron and its synaptic structures. The image stacks were first stitched together to make a larger single image using rigid translation based on the red fluorescence channel (Fig. 2*B*). Composite images acquired over 3 additional imaging sessions at 2- to 3-d intervals were then aligned to the baseline images by nonrigid warping of the red channel using procedures in the Computational Morphology Toolkit (CMTK) (38). Images acquired even 8 d apart were aligned by this procedure (Fig. 2*C*).

To measure large numbers of pre- and postsynaptic puncta, a custom ImageJ plugin was written for semiautomated puncta detection and measurement (Fig. 2*D* and *Methods*) (39). Because GFP expression is confined to synaptic sites, but was not present at detectable levels in our images of dendrites and axons, it appears as puncta in the green channel that are reliably detected using our algorithm. The detected puncta were then linked over days, based on criteria optimized either for post- or presynaptic markers (Fig. 2*D*). This high-throughput procedure, which allowed us to process the images to a reproducible and consistent standard, was in all cases followed by manual inspection to verify and make corrections when necessary.

MD Causes Bimodal Changes in Postsynaptic Densities. To examine the anatomical changes underlying the different stages of ocular dominance plasticity, we tracked the turnover of postsynaptic structures in layer 2/3 neurons through the critical period (~P28–P36), at intervals of 2 to 3 d (15, 16). We studied 4 control mice with normal visual experience for 8 d and 4 MD mice in which the contralateral eyelid was sutured closed for 6 d then reopened for the following 2 d. Previous physiological experiments showed that this procedure produces a progressive and robust ocular dominance shift that is reversed by the 2 d of binocular vision (15, 16). In the MD mice, the first 3 d of MD at the peak of the critical period caused a drastic change in the spine densities (Fig. 3*A*): many spines disappeared (marked by blue arrow) and few new spines formed (red arrow). Spine elimination was significantly increased (15.6 ± 1.8% in 3 d MD vs. 7.9 ± 0.6% in 3 d control,

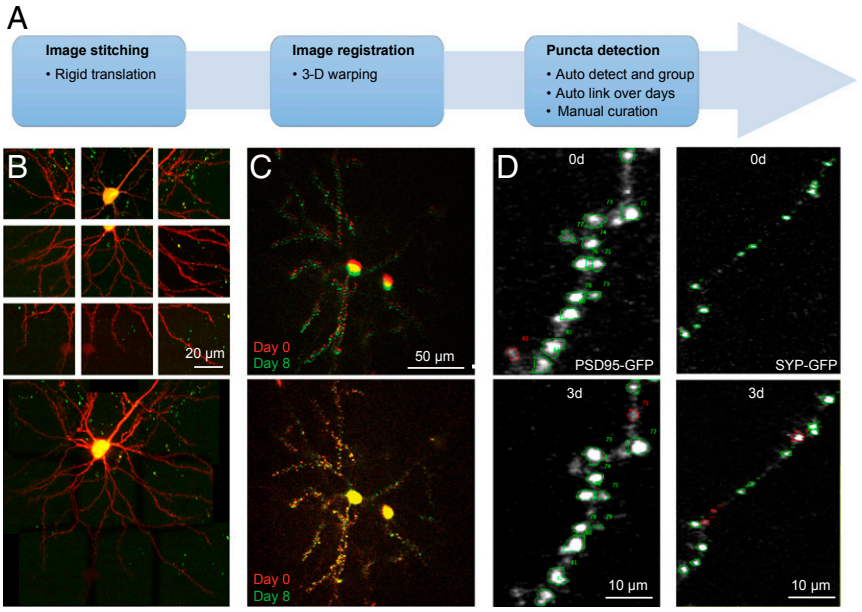

Fig. 2. Image processing pipeline and semiautomated puncta detection. (*A*) Image processing pipeline consists of 3 steps: image stitching, image registration, and semiautomatic puncta detection. (*B*) Nine high-resolution images were taken covering the region of interest (ROI) in a layer 2/3 excitatory neuron (*Top*), and automated 3D stitching using rigid translation was applied to obtain a single ROI (*Bottom*). (*C*) tdTomato channel images taken over days false colored in red and green and superimposed (*Top*) were aligned using 3D warping (nonrigid registration) to correct the misalignment caused by imaging acquisition as well as tissue growth (*Bottom*). (*D*) Automated detection and grouping of 3D puncta were performed by comparing ROIs over different days. Puncta detected over different days were automatically linked based on their spatial locations, followed by manual inspection to verify and make necessary correction. Examples of PSD95-GFP and SYP-GFP are shown, with green circle denoting the linked puncta and red circle denoting the unlinked ones.

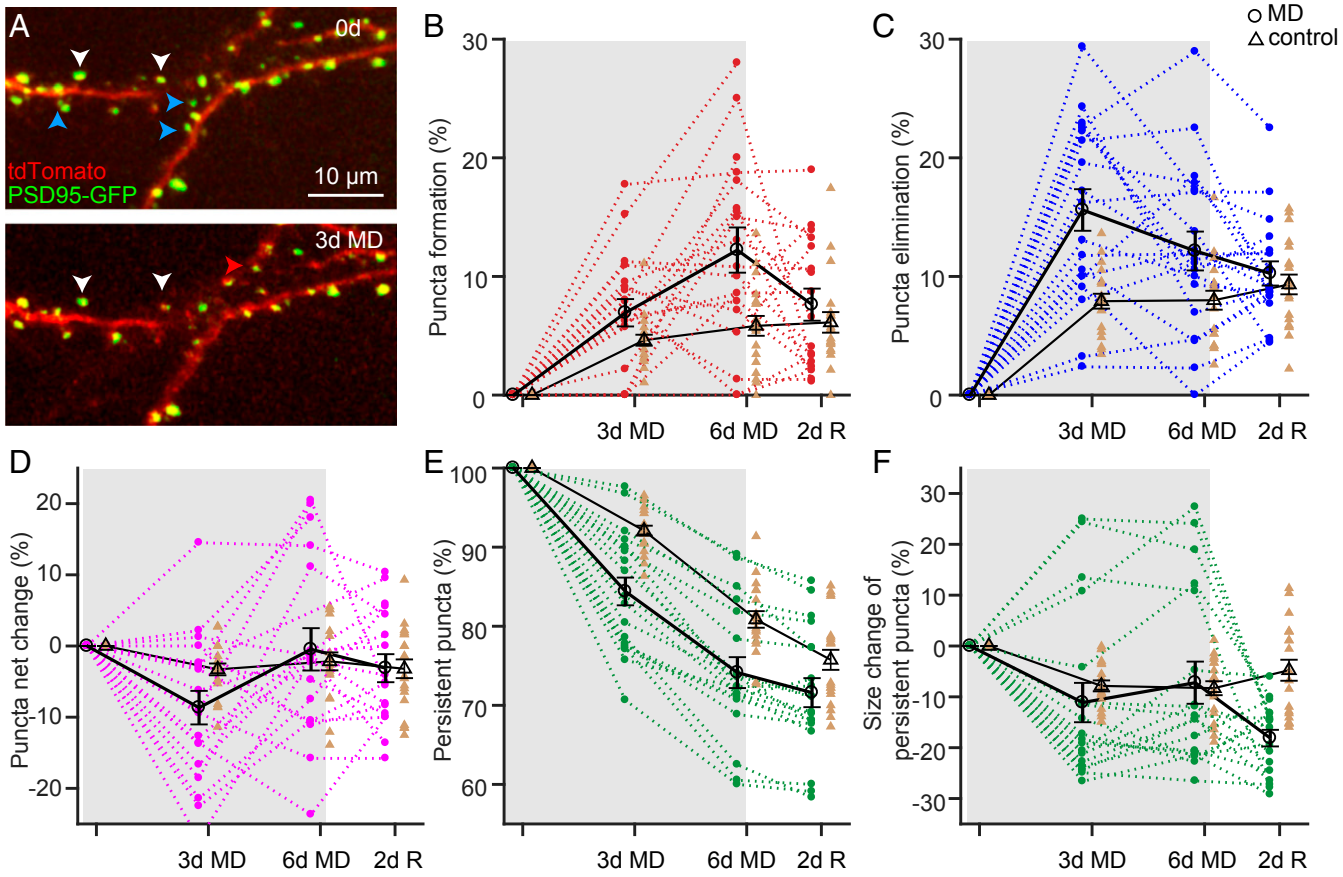

Fig. 3. Changes in postsynaptic densities of layer 2/3 neurons. (*A*) Postsynaptic marker PSD95-GFP coexpressed with tdTomato in a layer 2/3 excitatory neuron. White arrows mark persistent boutons, blue arrows mark lost bouton, and a red arrow marks new bouton. (*B–D*) Percentage change in dendritic spine formation, elimination, and total net change over 8 d in the binocular zone. (*E*) Fraction of persistent PSD95-GFP puncta throughout the period of MD and recovery. (*F*) Percentage change in size of persistent PSD95-GFP puncta. Each point marks the average value for the 18 to 54 spines on a single dendrite. Successive measurements of each dendrite in experimental animals connected by dotted lines. Average values for the 20 dendrites in 4 experimental animals indicated by open circles and heavy black line (627 puncta total). Control data are plotted in light brown; average values for the 19 dendrites in 4 control animals are indicated by open triangles connected by light black lines (711 puncta total).

$P < 0.0001$, $n = 20$ dendrites in 4 experimental animals, $n = 19$ dendrites in 4 control animals, unpaired Welch's t test) but there was only a modest, insignificant change in spine formation (6.9 ± 1.2% in 3 d MD vs. 4.6 ± 0.5% in 3 d control, $P = 0.066$). As a result, 3 d of MD caused a net loss of spines that was significantly larger than control (−8.7 ± 2.4% in 3 d MD vs. −3.3 ± 0.9% in 3 d control, $P = 0.035$). In contrast, spine elimination and formation were balanced over this period in the control animals (Fig. 3 *D–F*).

A delayed but significant increase in spine formation was evident by 6 d of MD (12.2 ± 2.0% in 6 d MD vs. 5.8 ± 0.9% in 6 d control, $P = 0.0035$), in addition to the spine elimination (12.1 ± 1.7% in 6 d MD vs. 8.0 ± 0.8% in 6 d control, $P = 0.029$). Consistent with the different direction of changes in the responses of neurons dominated by the deprived and nondeprived eyes (10), the net spine changes at 6 d of MD appear bimodal, with some dendritic branches losing many spines and others growing many (Fig. 3*D* and *Discussion*). This bimodality (or multimodality) was evident in that the different spine changes among the dendrites could no longer be fit by a normal distribution ($P = 0.0123$ in 6 d MD, $P = 0.26$ in 6 d control, Lilliefors test for normal distribution). The diversity of changes of spines among the dendrites was reversed by 2 d of binocular vision, resulting in a rate of spine elimination and formation similar to control animals (Fig. 3 *B–D*, elimination: 7.6 ± 1.4% in 2 d recovery vs. 6.1 ± 0.9% at the corresponding time in control mice; formation: 10.3 ± 1.0% in 2 d recovery vs. 9.3 ± 0.9% in control; net change: −3.1 ±2.0% in 2 d recovery vs. −3.2 ± 1.4% in control).

Over the 8 d of imaging, there were significantly fewer persistent puncta in MD mice than in control mice (84.4 ± 1.8% in 3 d MD vs. 92.1 ± 0.6% in 3 d control, $P = 0.0045$; 74.1 ± 2.0% in 6 d MD vs. 80.9 ± 1.1% in 6 d control, $P = 0.0223$, 2-way ANOVA corrected for multiple comparisons), indicating the altered visual experience destabilized the existing puncta (Fig. 3*E*). After 2 d of normal vision, this difference became insignificant (71.6 ± 1.9% in 2 d recovery vs. 75.8 ± 1.3% in 8 d control, $P = 0.3526$). The change in size of the persistent puncta (Fig. 3*F*) in the deprived mice also appears bimodal, with some puncta growing bigger while others became smaller ($P = 0.0061$ in 3 d MD, $P = 0.016$ in 6 d MD, $P = 0.5$ in 3 d control, $P = 0.49$ for 6 d control, Lilliefors test for normal distribution). Interestingly, restoration of normal vision for 2 d was sufficient for the enlarged puncta to revert to normal size, but not for the reduced puncta to recover, resulting in a net decrease in puncta size (−18.1 ± 1.7% in 2 d recovery vs. −4.8 ± 2.1% in 8 d control, $P = 0.0058$, 2-way ANOVA corrected for multiple comparisons).

Structural Changes of Postsynaptic Densities Correlate with Their Functional Responses. To elucidate the relationship between the anatomical changes and function during ocular dominance plasticity, we measured both in the same layer 2/3 excitatory neurons in 4 additional animals. We first examined the changes in dendritic

spines produced by MD by imaging neurons that coexpressed PSD95-GFP and tdTomato before and after 3 d of deprivation. After tracking the spine changes, we performed 2-photon calcium imaging to measure the functional responses in the same neurons. The calcium indicator Oregon Green Bapta-AM (OGB1) was applied to the binocular zone of V1 after removing the cover glass from the cranial window. Full-field drifting gratings were shown successively to the 2 eyes in order to elicit eye-specific visual responses. The responses at the preferred orientation for each cell were used to calculate the neuron's ocular dominance index (ODI) (Fig. 4*A*). Such structural and functional measurements revealed a strong correlation between the anatomical changes in spines and the eye-specific responses: dendrites of neurons more strongly dominated by the deprived eye (higher ODI) lost more PSD95-GFP puncta, while those of neurons in which responses to the 2 eyes were more nearly equal (lower ODI) lost fewer or gained puncta (Fig. 4*B*).

MD Reduces Formation of Presynaptic Boutons. We examined the turnover of presynaptic boutons within layer 2/3 in excitatory neurons of that layer that coexpressed SYP-GFP and tdTomato (Fig. 5*A*). In control mice, there was a steady, significant net increase in the number of presynaptic boutons until the peak of the critical period, followed by a return to baseline at the end of the critical period (Fig. 5 *B–D*, 6.3 ± 2.1% in 3 d control, 11.2 ± 3.1% in 6 d control, −3.5 ± 2.8% in 8 d control, $n = 24$ branches in 3 control animals, $P = 0.011$ for 3 d vs. baseline, $P < 0.001$ for 6 d vs. baseline, $P = 0.60$ for 8 d vs. baseline, ANOVA corrected for multiple comparisons).

In MD mice, 3 d of MD did not have a significant effect on bouton formation (10.2 ± 1.1% in 3 d MD vs. 11.7 ± 1.7% in 3 d control, $P = 0.34$, $n = 25$ branches in 4 experimental animals, $n = 24$ branches in 3 control animals, unpaired Welch's t test) or elimination (6.2 ± 0.6% in 3 d MD vs. 4.8 ± 0.7% in 3 d control, $P = 0.064$) compared to control. However, by 6 d of MD, bouton formation was significantly reduced from control (10.6 ± 1.2% in 6 d MD vs. 16.6 ± 2.5% in 6 d control, $P = 0.0035$), and bouton elimination was increased (7.4 ± 0.5% in 6 d MD vs. 5.5 ± 0.8% in 6 d control, $P = 0.0014$). Therefore, the net change in the numbers of presynaptic boutons was significantly affected by 6 d of MD (3.2 ± 1.4% in 6 d MD vs. 11.2 ± 3.1% in 6 d control, $P = 0.0019$) but not 3 d of MD (4.0 ± 1.4% in 3 d MD vs. 6.3 ± 2.1% in 3 d control, $P = 0.26$). This temporally restricted increase is consistent with a strengthening of synapses and the homeostatic scaling mechanisms demonstrated to occur between 3 and 6 d of MD (16). Notably, MD did not have a significant effect on persistent boutons (Fig. 5 *E* and *F*).

Discussion

Previous physiological studies of ocular dominance plasticity have focused on the cortical neurons in the thalamorecipient layer 4 as well as the layers above and below (reviewed in refs. 3, 6, and 40). However, studies of structural plasticity in vivo during the critical period have focused on the spines of apical dendrites in layer 1, in most cases from pyramidal neurons in layer 5 (37, 41). The physiological changes in these neurons were generally not characterized, making it difficult to determine the extent to which the time course of the structural changes was consistent with physiological plasticity and might therefore underlie it.

The present study examines both postsynaptic and presynaptic structures in axons and dendrites of layer 2/3 excitatory neurons, in which the time course of ocular dominance plasticity and underlying signaling mechanisms have been the subject of many reports (reviewed in ref. 6). To investigate the anatomical substrates that underlie the ocular dominance plasticity, we tracked the gains and losses of presynaptic boutons and postsynaptic densities in individual neurons in the binocular zone of mouse visual cortex during the critical period. We labeled major proteins of dendritic spines (PSD95) and presynaptic boutons (SYP) in individual layer 2/3 neurons and followed them through 6 d of monocular deprivation during the peak of the critical period plus 2 d of recovery with binocular vision, the same deprivation and recovery protocol that was used for the studies of cellular signaling mechanisms (15, 16). To determine whether the anatomical changes corresponded with eye-specific visual responsiveness in individual neurons, we applied calcium imaging to measure the physiological effects of MD in neurons after measuring their anatomical changes. Our findings suggest that the rapid anatomical rewiring of intracortical connections serves as a structural basis for the physiological effects of monocular deprivation in these layer 2/3 neurons.

Measuring Structural Changes in Synapses below Layer 1. Measuring changes in synaptic structures below the most superficial layer of the cortex using optical microscopy is challenging even with 2-photon microscopy. Because the best possible axial resolution is comparable to the size of the smaller dendritic spines, the presence of the fluorophore within both dendrite and spine may artifactually cause the spine to disappear or reappear when the size or orientation of a spine, or the clarity of the tissue, changes across imaging sessions. The use of fluorescent label for the major protein of the postsynaptic density (PSD95) produces discrete puncta in the image that can be counted unambiguously and measured accurately, independent of the inevitable changes in optical resolution within deeper cortical layers over days.

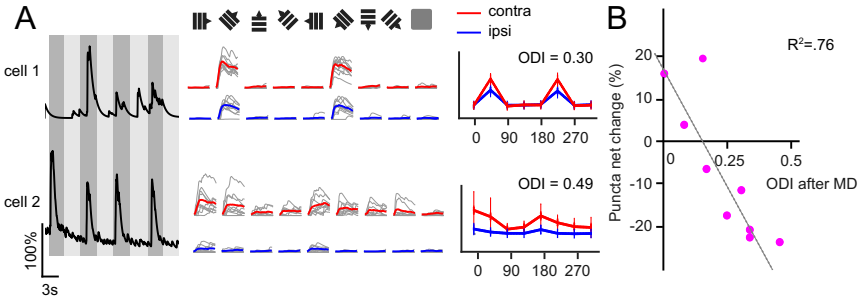

Fig. 4. Relationship of ocular dominance in single layer 2/3 neurons to postsynaptic structural changes during MD. (*A*) Functional imaging after structural imaging following 3 d of MD in a separate group of 4 animals. Full-field drifting gratings of 8 different orientations presented to left and right eyes to evoke eye-specific responses. Averaged response at the preferred orientation was used to calculate the ocular dominance index in each neuron. (*B*) The loss/gain of postsynaptic density marker PSD95-GFP in each neuron was strongly correlated with the ocular dominance index ($r^2 = 0.76$), 9 neurons with 143 to 1,123 puncta per neuron.

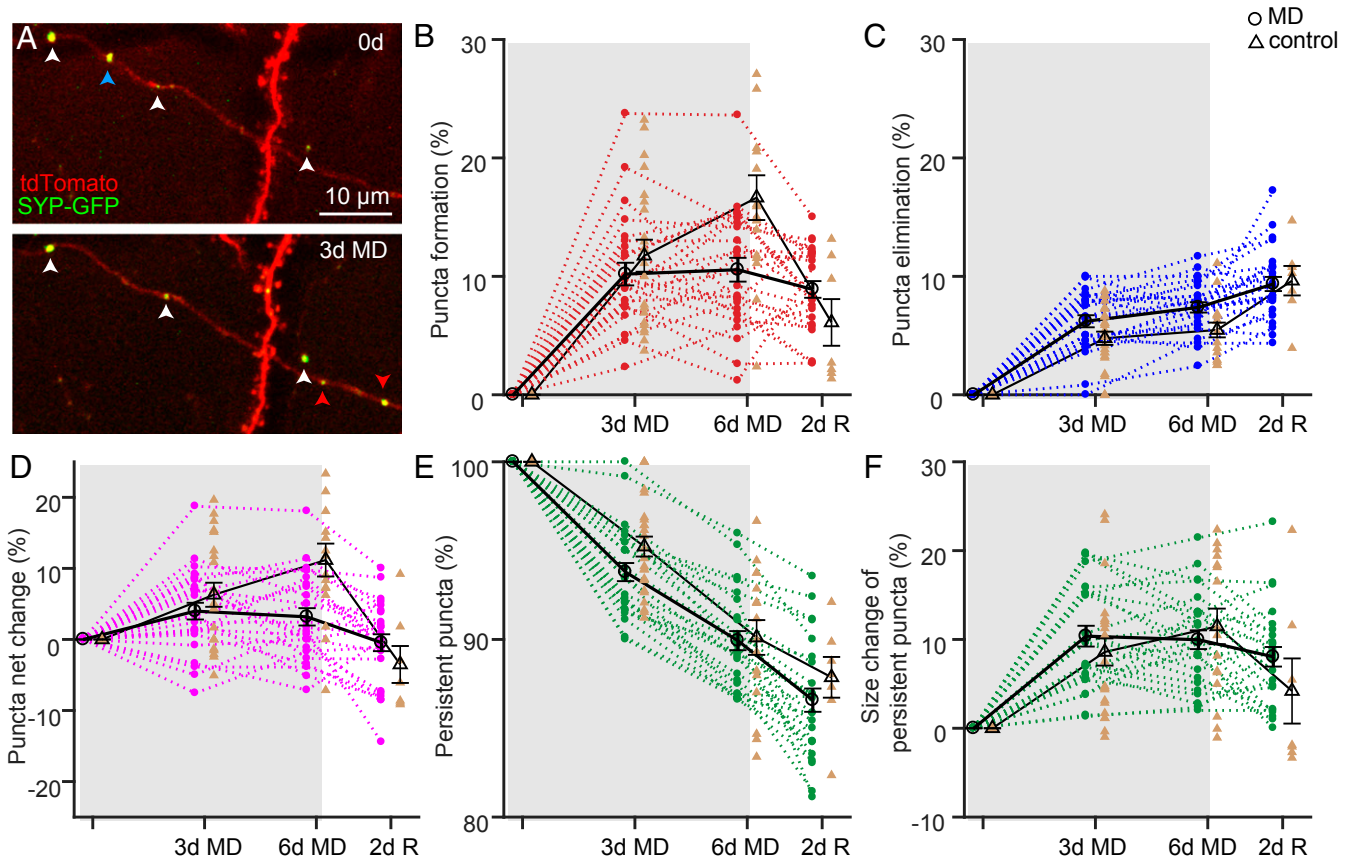

Fig. 5. Changes in presynaptic boutons of layer 2/3 neurons. (*A*) Presynaptic marker SYP-GFP coexpressed with tdTomato in a layer 2/3 excitatory neuron. White arrows mark persistent boutons, red arrows mark gain of boutons, and a blue arrow marks loss of a bouton. (*B–D*) Percentage change in bouton formation, elimination, and total net change over 8 d in the binocular zone. (*E*) Fraction of persistent SYP-GFP puncta throughout the period of MD and recovery. (*F*) Percentage change in size of persistent SYP-GFP puncta. Each point marks the average value for the 17 to 61 boutons on a single axonal branch. Successive measurements of each branch in experimental animals connected by dotted lines. Average values for the 25 branches in 4 experimental animals are indicated by open circles and heavy black line (864 boutons total). Control data are plotted in light brown; average values for the 24 branches in 3 control animals are indicated by open triangles connected by light black lines (727 boutons total).

Overexpression of PSD95 is known to alter synaptic plasticity both in hippocampus and cerebral cortex (42–46). While our aim was to deliver only tracer amounts of fluorescent protein that would have no effect on plasticity, control experiments were required to exclude such an effect. We performed these by measuring cortical plasticity in vivo after delivering a much higher concentration of PSD95-GFP plasmid with much wider expression than was used in the actual experiments, and we found that the response to monocular deprivation was normal (Fig. 1*G*).

The resolution of presynaptic boutons in optical microscopy is even more difficult than for dendritic spines because not all swellings of an axon are presynaptic sites. To count and measure presynaptic terminals we labeled synaptophysin, a major presynaptic protein essential for synaptic vesicle release (47–49). SYP-GFP appears as discrete puncta along axons in 2-photon microscopy (Figs. 1 and 5). As with PSD95-GFP, even much greater expression of SYP-GFP in a wider population than was used in the experimental cases did not affect normal ocular dominance plasticity (Fig. 1*I*).

Reorganization at Layer 2/3 Postsynaptic Sites Closely Follows Functional Changes. Ocular dominance plasticity during early development takes places in 3 stages with distinctive physiological changes in layer 2/3 neurons in the binocular zone of V1 (Fig. 6*A*): 1) a dramatic loss of response to the deprived eye; 2) a significant increase in open eye response and a slight increase in deprived eye response; and 3) a return of responses to their initial state after reopening the deprived eye (reviewed in ref. 6).

The present study finds that structural changes in postsynaptic spines have a similar time course and direction of change to physiological ocular dominance plasticity (Fig. 6 *B* and *C*). After 3 d of MD, there was a significant loss of spine number due to greater spine elimination. By 6 d of MD, there was more spine formation and less elimination, resulting in a small net change in spine numbers averaged over all of the dendrites, but the changes in individual dendrites became so diverse that they could no longer be fit by a normal distribution. The sizes of persistent puncta also became very diverse at both 3 and 6 d of MD, suggesting that enlargement of some of the existing puncta precedes the formation of new spines in response to altered visual inputs. Restoration of binocular vision for 2 d quickly brought back these diverse changes to a normal distribution in size and number.

The neurons in which calcium imaging of visual responses was carried out following structural measurement demonstrated a strong correlation between each neuron's spine remodeling and physiological responses to the 2 eyes. Previous studies have demonstrated that spines from the same dendritic tree tend to share the same orientation preference, while different dendritic segments from the same neuron are biased toward different orientations (50). If inputs to individual dendrites were also eye specific, then MD would be expected to produce diverse changes in spine number and size on different dendrites, as we observed

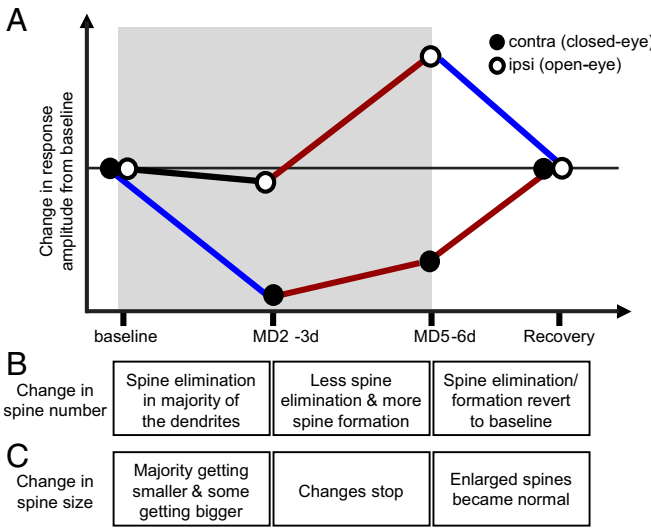

Fig. 6. Stages of ocular dominance plasticity during the critical period. (*A*) Ocular dominance plasticity takes place in temporally and mechanistically distinct stages: a decreased response to the deprived eye in the first 2 to 3 d, a delayed increase in response to the open eye, and a full recovery in 2 d of normal vision. (*B*) Change in spine number has comparable time course and direction: loss of spines by 3 d of MD, decreased spine elimination and increased spine formation by 6 d of MD, and a full recovery to baseline after 2 d of binocular vision. (*C*) Change in the size of persistent spines reacts faster to MD: the majority of dendrites has decreased spine size and some dendrites have increased spine sizes by 3 d of MD, and no further change by 6 d of MD. Enlarged spines become normal after restoration of normal vision.

(Fig. 3*D*). The gains and losses of PSD95-GFP puncta in individual dendrites of deprived animals showed a tendency toward anticorrelation that did not reach statistical significance. Our functional imaging using OGB1-AM, while revealing somatic responses, was not capable of resolving dendritic signals. It will be interesting for future studies to explore potential dendritic specificity for ocular dominance.

Our findings of changes in spines of individual neurons are consistent with population studies of developing visual cortex showing decreased spine density after visual deprivation by MD (36, 37) or dark rearing (34, 35). A number of studies (33, 35, 36) have shown correlations between anatomical and functional changes at the population level consistent with our demonstration of a relationship between anatomical change and eye-specific responses at single cells. The rapid remodeling, including changes in number and size of spines, and the correlation between structural and functional changes in individual cells observed in the present study suggest that these changes may be the cellular substrate for functional reorganization during experience-dependent plasticity in the developing mouse V1 (Fig. 6).

Delayed Reorganization of Layer 2/3 Presynaptic Boutons during the Critical Period. Control mice receiving normal visual inputs showed a steady increase of presynaptic bouton number during the critical period, whereas the number of postsynaptic spines in control animals remained stable during this period. It is worth noting that, while we specifically labeled presynaptic and postsynaptic structures in layer 2/3 excitatory neurons, the synaptic markers used, SYP-GFP and PSD95-GFP, do not target the same types of synapses: PSD95-GFP puncta receive excitatory inputs, principally from layer 2/3 and layer 4 excitatory neurons, though these spines may also receive some degree of inhibition. On the other hand, the presynaptic structures labeled by SYP-GFP target inhibitory as well as excitatory neurons, both within layer 2/3 and possibly onto the dendrites of neurons in other layers. Structural changes in the presynaptic outputs from layer 2/3 cells, unlike those in their postsynaptic inputs, might therefore not be expected to match the changes in their visual responses. These differences may explain why the effect of MD on the presynaptic boutons in the cells examined was smaller and slower than the changes at postsynaptic spines.

Many studies have shown that maturation of inhibitory neurons at the end of the critical period is involved in critical period plasticity (3, 40, 51). The increase in bouton formation at the end of the critical period when spine number on the excitatory neurons remains stable suggests an increase of excitatory inputs onto local inhibitory neurons, which may contribute to the end of the critical period. In the adult visual cortex, 2-photon microscopy of gephyrin-labeled inhibitory synapses show them to be highly dynamic, being removed and replaced repeatedly at the same sites, in contrast to the relatively stable excitatory synapses (32). Adult ocular dominance plasticity is associated with a specific loss of inhibitory inputs (29, 30). It will be interesting to apply similar techniques to measure the turnover of inhibitory synapses during the critical period.

Methods

Experimental Animals. All animal work was approved by the University of California San Francisco (UCSF) Animal Care and Use Program and conforms to the National Institutes of Health guidelines. Ai14 (stock No. 007908, The Jackson Laboratory), and wild-type C57BL/6J (Charles River, CA) lines were purchased to breed and maintain in the UCSF housing facility, on a standard 12 h dark/light cycle. Both sexes of animals were included in the study.

DNA Constructs and In Utero Electroporation. The 4 plasmids used in our present study were pCAG-Cre (Addgene plasmid 13775), pEF1a-double flox-PSD95-eGFP-WPRE (Addgene plasmid 133785), pCAG-double floxed-SYP-eGFP-WPRE (Addgene plasmid 73816), and pEF1a-double-floxed-tdTomato-WPRE (Addgene plasmid 133786). The latter 3 were generated by subcloning original constructs and then customizing them into specific promoters (available in Addgene for distribution). Plasmids were delivered through in utero electroporation as previously described (52, 53) to E16 Ai14 mouse embryos to label layer 2/3 cortical excitatory neurons. Pregnant female mice were anesthetized with isoflurane (3% for induction and 1.5% for maintenance) with injection of Buprenex (0.1 mg/kg) and carprofen (15 mg/kg). After laparotomy, ~1 μL of a solution consisting of artificial cerebrospinal fluid (ACSF), 0.1% of Fast Green (Sigma-Aldrich, St. Louis, MO), pCAG-Cre (0.0001 μg/μL), 1 type of double flox marker for PSD95 or SYP (0.75 μg/μL), and double-floxed tdTomato (0.75 μg/μL) was injected into the left ventricle of each embryo through a glass capillary with a tip diameter of 20 to 30 μm (Drummond Scientific, Broomall, PA). A pair of platinum electrodes positioned to target the dorsolateral wall of the left hemisphere and a series of 5 square-wave current pulses (35 V, 50-ms duration, 950-ms interval) were delivered by a pulse generator (ECM830; BTX, San Diego, CA). Afterward, embryos were put back into the mother's womb, which was then closed by sutures for normal delivery and growth.

Headplate and Cranial Window Implantation. For long-term visualization of neuronal morphology under a 2-photon microscope, animals at P22–25 (4 to 5 d before imaging) were implanted with a stainless headplate and a cranial window was made as previously described (54–56). Briefly, animals were anesthetized with isoflurane (3% induction; 1.5% surgery), and injected s.c. with atropine (0.15 mg/kg), dexamethasone (1.5 mg/kg), and carprofen (15 mg/kg). After a scalp incision and fascia cleaning, a customized stainless steel headplate was secured to the skull with cyanoacrylate glue (VetBond, 3M) and dental acrylic (Lang Dental Black Ortho-Jet powder and liquid). A craniotomy was made with steel drill bits centered approximately on the binocular zone of the visual cortex (3 mm lateral to midline, 1 mm anterior to lambda); gel foam soaked in ACSF was used to cover the exposed cortical area for 5 min; and a 3-mm-diameter circular glass coverslip was secured using cyanoacrylate.

Intrinsic Signal Imaging. Binocular V1 was functionally located by brief transcranial intrinsic signal imaging as previously described (15, 57). To evoke robust visual responses, mice were injected with chlorprothixene (2 mg/kg, i.m.) and anesthesia was maintained using a low concentration of isoflurane (0.6 to 0.8% in oxygen); the core body temperature was maintained at 37.5° using a feedback heating system. A temporally periodic moving 2°-wide bar was generated using the Psychophysics Toolbox (58, 59) in

Matlab (Mathworks) and continuously presented at a speed of 10°/s. To identify binocular V1, the visual stimulus subtended 20° horizontal and was presented to 1 eye at a time (the nontested eye blocked with eye shutter) with monitor positioned directly in front of the animal. To calculate ODI, response amplitude was averaged from at least 4 measurements, and ODI was computed as $(R - L)/(R + L)$, where R and L are the peak response amplitudes through the right eye and the left eye, respectively, using a custom Matlab code (60).

Monocular Deprivation. Monocular deprivation was induced by suturing the right eyelid with 7-0 polypropylene monofilament (Ethicon). Suture integrity was inspected immediately prior to each imaging session. Animals whose eyelids did not seal fully shut or had accidentally reopened were excluded from further experiments.

Two-Photon Imaging. Two-photon imaging was performed using a movable objective microscope manufactured by the Sutter Instrument Company. A mode-locked Ti:Sapphire laser (Chameleon Ultra 2, Coherent, Inc.) was tuned to 910–950 nm, and the laser power through the objective was adjusted within the range of 50 to 100 mW. Emission light was collected by a 40× water-immersion objective (NA0.8; IR2; Olympus), filtered by emission filters (525/70 and 610/75 nm; Chroma Technology) and measured by 2 independent photomultiplier tubes (Hamamatsu R3896). Scanning and image acquisition was controlled by ScanImage software (Vidrio Technologies). Mice were anesthetized with isoflurane and head fixed for structural and functional imaging.

Imaging Processing Pipeline and Semiautomated Puncta Detection. Segmented images from the same imaging sessions were first stitched using linear transformation, and the composite images from different imaging sessions were further aligned by rigid translation followed by 3-dimensional warping (38). To compare GFP-tagged synaptic structures across imaging sessions, a customized and semiautomated ImageJ plugin (deposited at https://github.com/ucsfidl/Puncta_Counter) was used to outline and group the 2-dimensional boundaries of individual puncta to create 3-dimensional boundaries. Identified puncta had to be a minimal size of $2 \times 2 \times 2$ or 8 clustered pixels with a minimal average signal intensity of at least 3 times above shot-noise background level, consistent with synapses of these pixel dimensions correlating to their true physical dimensions as measured after electron microscopic reconstruction (29). Using these criteria, the software automatically identifies and outlines at least 95% of puncta, with almost no false positive identification of background noise or ascending neurite branches. Less than 1% of 2 or more puncta are interpreted as 1, and less than 1% of single puncta are interpreted as 2.

Individual puncta are given a unique identification number and a number corresponding to cell of origin identified by using tdTomato neurite labeling. Following the identification and outlining of puncta, the position and pixel volume (total number of pixels) were calculated. Stable synaptic structures were defined as those identified in all imaging sessions. Dynamic synapses were defined as puncta that appeared or disappeared for 1 or more imaging sessions.

Axonal or basal dendritic branches containing at least 15 PSD95-GFP or SYP-GFP puncta within a 40-μm range of depth were selected for analysis. This plane included the soma in the case of the dendrites. Changes in puncta numbers were measured from the baseline images. The net change was calculated as the numbers of puncta added, minus those eliminated, divided by the baseline numbers. Puncta were counted as persistent if they were continuously present from the baseline images.

Calcium Imaging and Data Analysis. In a separate group of animals, we also measured the visual responses of the neurons that underwent structural imaging to correlate the functional and anatomical relationship. To obtain functional responses of the labeled neurons, calcium-sensitive dye OGB1-AM (Molecular Probes) was applied after structural imaging. The glass coverslip over the cranial window was carefully removed with fine forceps after drilling off dental acrylic. As previously described (61), OGB1-AM (dissolved in DMSO containing 20% Pluronic F-127 and further diluted 1:10 in bath solution 50 NaCl, 2.5 KCl, 10 Hepes, pH 7.4) was slowly injected into the binocular zone under constant pressure of ~10 psi (Picospritzer, general valve) for ~1 min at a depth of 150 to 300 μm through a pipette with a tip size of ~2 μm (inside diameter). The progress of administration was visualized by inclusion of a nontoxic red fluorescence dye, Alexa 594 (Invitrogen). Typically, 3 injections were made to cover the binocular zone.

To measure the eye-specific responses under a 2-photon microscope, 2.5% agarose in ACSF was applied over the brain and sealed with a coverslip and petroleum jelly. A preanesthetic injection of chlorprothixene (2 mg/kg, i.m.) and 0.7% isoflurane was applied to allow robust visual responses. Full-field drifting sinusoidal gratings (0.04 cycles per degree [cpd], 99% contrast, 1 Hz temporal frequency) at 8 evenly spaced directions were generated and presented for 3 s, separated by 3-s blank periods of uniform 50% gray, in random sequence using the Matlab Psychophysics Toolbox (58, 59). Stimuli to the 2 eyes were randomly interleaved using a pneumatic shutter and the stimulus sequence was presented 5 times, randomizing the order between presentations. Independent component analysis was then used to extract somatic calcium transients as a measure for cellular visual responses (62). To calculate ODI, response amplitude was averaged from at least 4 measurements, and ODI was computed as $(R_p - L_p)/(R_p + L_p)$, where R_p and L_p were the peak response amplitudes at the preferred orientation through the right eye and the left eye, respectively.

Statistical Analysis. Distribution of group data was tested for normality using the Lilliefors test. Only data that passed normality test were presented as mean ± SEM. For comparison between experimental and control groups, unpaired Welch's (unequal variance) *t* test was conducted with *P* value reported. For comparison of change in the same branches between experimental and control groups over days, unbalanced 2-way ANOVA was conducted, followed by post hoc tests using Tukey's method, and the adjusted *P* value was reported. For function and structure relationship, regression was performed using Matlab linear least squares fitting, with adjusted R-squared reported.

ACKNOWLEDGMENTS. We thank Drs. K. Svoboda (PSD95), S. Arber (Synaptophysin), K. Deisseroth (double flox), and Linda Willbrecht and Denise Niell (double-floxed PDS95-eGFP) for the original constructs and R. Mostany, C. Portera-Cailliau, and V. Cairone for technical consultation. We thank members of the M.P.S. laboratory for helpful discussion, particularly M. Kaneko, S. Gandhi, and C. Niell for assistance and training on in utero electroporation and calcium imaging. This work was supported by grants from the NIH R01EY02874 (to M.P.S.), K22NS089799 (to J.S.E.), and K99EY029002 (to Y.J.S.).

1. M. Inan, M. C. Crair, Development of cortical maps: Perspectives from the barrel cortex. *Neuroscientist* **13**, 49–61 (2007).
2. L. I. Zhang, S. Bao, M. M. Merzenich, Persistent and specific influences of early acoustic environments on primary auditory cortex. *Nat. Neurosci.* **4**, 1123–1130 (2001).
3. T. K. Hensch, Critical period plasticity in local cortical circuits. *Nat. Rev. Neurosci.* **6**, 877–888 (2005).
4. B. S. Wang, R. Sarnaik, J. Cang, Critical period plasticity matches binocular orientation preference in the visual cortex. *Neuron* **65**, 246–256 (2010).
5. A. J. King, D. R. Moore, Plasticity of auditory maps in the brain. *Trends Neurosci.* **14**, 31–37 (1991).
6. J. S. Espinosa, M. P. Stryker, Development and plasticity of the primary visual cortex. *Neuron* **75**, 230–249 (2012).
7. D. E. Feldman, M. Brecht, Map plasticity in somatosensory cortex. *Science* **310**, 810–815 (2005).
8. T. N. Wiesel, D. H. Hubel, Single-cell responses in striate cortex of kittens deprived of vision in one eye. *J. Neurophysiol.* **26**, 1003–1017 (1963).
9. N. P. Issa, J. T. Trachtenberg, B. Chapman, K. R. Zahs, M. P. Stryker, The critical period for ocular dominance plasticity in the Ferret's visual cortex. *J. Neurosci.* **19**, 6965–6978 (1999).
10. J. A. Gordon, M. P. Stryker, Experience-dependent plasticity of binocular responses in the primary visual cortex of the mouse. *J. Neurosci.* **16**, 3274–3286 (1996).
11. M. Y. Frenkel, M. F. Bear, How monocular deprivation shifts ocular dominance in visual cortex of young mice. *Neuron* **44**, 917–923 (2004).
12. J. C. Horton, D. R. Hocking, Timing of the critical period for plasticity of ocular dominance columns in macaque striate cortex. *J. Neurosci.* **17**, 3684–3709 (1997).
13. B. J. Yoon, G. B. Smith, A. J. Heynen, R. L. Neve, M. F. Bear, Essential role for a long-term depression mechanism in ocular dominance plasticity. *Proc. Natl. Acad. Sci. U.S.A.* **106**, 9860–9865 (2009).
14. T. D. Mrsic-Flogel *et al.*, Homeostatic regulation of eye-specific responses in visual cortex during ocular dominance plasticity. *Neuron* **54**, 961–972 (2007).
15. M. Kaneko, J. L. Hanover, P. M. England, M. P. Stryker, TrkB kinase is required for recovery, but not loss, of cortical responses following monocular deprivation. *Nat. Neurosci.* **11**, 497–504 (2008).
16. M. Kaneko, D. Stellwagen, R. C. Malenka, M. P. Stryker, Tumor necrosis factor-α mediates one component of competitive, experience-dependent plasticity in developing visual cortex. *Neuron* **58**, 673–680 (2008).
17. K. K. A. Cho, L. Khibnik, B. D. Philpot, M. F. Bear, The ratio of NR2A/B NMDA receptor subunits determines the qualities of ocular dominance plasticity in visual cortex. *Proc. Natl. Acad. Sci. U.S.A.* **106**, 5377–5382 (2009).
18. D. E. Mitchell, F. Sengpiel, Neural mechanisms of recovery following early visual deprivation. *Philos. Trans. R. Soc. Lond. B Biol. Sci.* **364**, 383–398 (2009).
19. T. Rose, J. Jaepel, M. Hübener, T. Bonhoeffer, Cell-specific restoration of stimulus preference after monocular deprivation in the visual cortex. *Science* **352**, 1319–1322 (2016).
20. M. A. Silver, M. P. Stryker, Synaptic density in geniculocortical afferents remains constant after monocular deprivation in the cat. *J. Neurosci.* **19**, 10829–10842 (1999).

21. R. W. Guillery, D. J. Stelzner, The differential effects of unilateral lid closure upon the monocular and binocular segments of the dorsal lateral geniculate nucleus in the cat. *J. Comp. Neurol.* **139**, 413–421 (1970).
22. A. Antonini, M. P. Stryker, Rapid remodeling of axonal arbors in the visual cortex. *Science* **260**, 1819–1821 (1993).
23. C. J. Shatz, M. P. Stryker, Ocular dominance in layer IV of the cat's visual cortex and the effects of monocular deprivation. *J. Physiol.* **281**, 267–283 (1978).
24. A. Antonini, M. Fagiolini, M. P. Stryker, Anatomical correlates of functional plasticity in mouse visual cortex. *J. Neurosci.* **19**, 4388–4406 (1999).
25. J. T. Trachtenberg, C. Trepel, M. P. Stryker, Rapid extragranular plasticity in the absence of thalamocortical plasticity in the developing primary visual cortex. *Science* **287**, 2029–2032 (2000).
26. J. T. Trachtenberg, M. P. Stryker, Rapid anatomical plasticity of horizontal connections in the developing visual cortex. *J. Neurosci.* **21**, 3476–3482 (2001).
27. A. J. G. D. Holtmaat *et al*., Transient and persistent dendritic spines in the neocortex in vivo. *Neuron* **45**, 279–291 (2005).
28. T. Keck *et al*., Massive restructuring of neuronal circuits during functional reorganization of adult visual cortex. *Nat. Neurosci.* **11**, 1162–1167 (2008).
29. J. L. Chen *et al*., Clustered dynamics of inhibitory synapses and dendritic spines in the adult neocortex. *Neuron* **74**, 361–373 (2012).
30. D. van Versendaal *et al*., Elimination of inhibitory synapses is a major component of adult ocular dominance plasticity. *Neuron* **74**, 374–383 (2012).
31. J. L. Chen, E. Nedivi, Highly specific structural plasticity of inhibitory circuits in the adult neocortex. *Neuroscientist* **19**, 384–393 (2013).
32. K. L. Villa *et al*., Inhibitory synapses are repeatedly assembled and removed at persistent sites in vivo. *Neuron* **90**, 662–664 (2016).
33. J. Grutzendler, N. Kasthuri, W. B. Gan, Long-term dendritic spine stability in the adult cortex. *Nature* **420**, 812–816 (2002).
34. W. Wallace, M. F. Bear, A morphological correlate of synaptic scaling in visual cortex. *J. Neurosci.* **24**, 6928–6938 (2004).
35. D. Tropea, A. K. Majewska, R. Garcia, M. Sur, Structural dynamics of synapses in vivo correlate with functional changes during experience-dependent plasticity in visual cortex. *J. Neurosci.* **30**, 11086–11095 (2010).
36. H. Yu, A. K. Majewska, M. Sur, Rapid experience-dependent plasticity of synapse function and structure in ferret visual cortex in vivo. *Proc. Natl. Acad. Sci. U.S.A.* **108**, 21235–21240 (2011).
37. Y. Zhou, B. Lai, W. B. Gan, Monocular deprivation induces dendritic spine elimination in the developing mouse visual cortex. *Sci. Rep.* **7**, 4977 (2017).
38. T. Rohlfing, C. R. Maurer, Jr, Nonrigid image registration in shared-memory multiprocessor environments with application to brains, breasts, and bees. *IEEE Trans. Inf. Technol. Biomed.* **7**, 16–25 (2003).
39. Y. J. Sun, Puncta_Counter. Github. https://github.com/ucsfidl/Puncta_Counter. Deposited 20 August 2019.
40. C. N. Levelt, M. Hübener, Critical-period plasticity in the visual cortex. *Annu. Rev. Neurosci.* **35**, 309–330 (2012).
41. A. K. Majewska, J. R. Newton, M. Sur, Remodeling of synaptic structure in sensory cortical areas in vivo. *J. Neurosci.* **26**, 3021–3029 (2006).
42. A. E. El-Husseini, E. Schnell, D. M. Chetkovich, R. A. Nicoll, D. S. Bredt, PSD-95 involvement in maturation of excitatory synapses. *Science* **290**, 1364–1368 (2000).
43. V. Stein, D. R. C. House, D. S. Bredt, R. A. Nicoll, Postsynaptic density-95 mimics and occludes hippocampal long-term potentiation and enhances long-term depression. *J. Neurosci.* **23**, 5503–5506 (2003).
44. I. Ehrlich, R. Malinow, Postsynaptic density 95 controls AMPA receptor incorporation during long-term potentiation and experience-driven synaptic plasticity. *J. Neurosci.* **24**, 916–927 (2004).
45. K. Futai *et al*., Retrograde modulation of presynaptic release probability through signaling mediated by PSD-95-neuroligin. *Nat. Neurosci.* **10**, 186–195 (2007).
46. X. Huang *et al*., Progressive maturation of silent synapses governs the duration of a critical period. *Proc. Natl. Acad. Sci. U.S.A.* **112**, E3131–E3140 (2015).
47. T. C. Südhof, F. Lottspeich, P. Greengard, E. Mehl, R. Jahn, A synaptic vesicle protein with a novel cytoplasmic domain and four transmembrane regions. *Science* **238**, 1142–1144 (1987).
48. L. Thomas *et al*., Identification of synaptophysin as a hexameric channel protein of the synaptic vesicle membrane. *Science* **242**, 1050–1053 (1988).
49. J. Alder, B. Lu, F. Valtorta, P. Greengard, M. M. Poo, Calcium-dependent transmitter secretion reconstituted in Xenopus oocytes: Requirement for synaptophysin. *Science* **257**, 657–661 (1992).
50. H. Jia, N. L. Rochefort, X. Chen, A. Konnerth, Dendritic organization of sensory input to cortical neurons in vivo. *Nature* **464**, 1307–1312 (2010).
51. H. Morishita, T. K. Hensch, Critical period revisited: Impact on vision. *Curr. Opin. Neurobiol.* **18**, 101–107 (2008).
52. T. Saito, N. Nakatsuji, Efficient gene transfer into the embryonic mouse brain using in vivo electroporation. *Dev. Biol.* **240**, 237–246 (2001).
53. H. Tabata, K. Nakajima, Labeling embryonic mouse central nervous system cells by in utero electroporation. *Dev. Growth Differ.* **50**, 507–511 (2008).
54. Y. Fu *et al*., A cortical circuit for gain control by behavioral state. *Cell* **156**, 1139–1152 (2014).
55. M. Kaneko, Y. Fu, M. P. Stryker, Locomotion induces stimulus-specific response enhancement in adult visual cortex. *J. Neurosci.* **37**, 3532–3543 (2017).
56. J. T. Trachtenberg *et al*., Long-term in vivo imaging of experience-dependent synaptic plasticity in adult cortex. *Nature* **420**, 788–794 (2002).
57. V. A. Kalatsky, M. P. Stryker, New paradigm for optical imaging: Temporally encoded maps of intrinsic signal. *Neuron* **38**, 529–545 (2003).
58. D. H. Brainard, The Psychophysics Toolbox. *Spat. Vis.* **10**, 433–436 (1997).
59. M. Kleiner *et al*., What's new in Psychtoolbox-3? *Cogn. Comput. Psychophys.* **36**, 1–89 (2007).
60. J. Cang, V. A. Kalatsky, S. Löwel, M. P. Stryker, Optical imaging of the intrinsic signal as a measure of cortical plasticity in the mouse. *Vis. Neurosci.* **22**, 685–691 (2005).
61. S. P. Gandhi, Y. Yanagawa, M. P. Stryker, Delayed plasticity of inhibitory neurons in developing visual cortex. *Proc. Natl. Acad. Sci. U.S.A.* **105**, 16797–16802 (2008).
62. K. Ohki, S. Chung, Y. H. Ch'ng, P. Kara, R. C. Reid, Functional imaging with cellular resolution reveals precise micro-architecture in visual cortex. *Nature* **433**, 597–603 (2005).